Chemistry–A European Journal

Synthesis, Characterization, and Catalytic Application of Colloidal and Supported Manganese Nanoparticles

Johannes Zenner, Kelly Tran, Liqun Kang, Niklas W. Kinzel, Christophe Werlé, Serena DeBeer, Alexis Bordet,* and Walter Leitner*

WILEY-VCH

Synthesis, Characterization and Catalytic Application of Colloidal and Supported Mn Nanoparticles

Johannes Zenner[ab], Kelly Tran[ab], Liqun Kang[a], Niklas W. Kinzel[ab], Christophe Werlé[ac], Serena DeBeer[a], Alexis Bordet[a]* and Walter Leitner[ab]*

*Correspondence:

Prof. W. Leitner
E-mail: walter.leitner@cec.mpg.de

Dr. A. Bordet
E-Mail: alexis.bordet@cec.mpg.de

[a]Max Planck Institute for Chemical Energy Conversion, Stiftstr. 34-36, 45470 Mülheim an der Ruhr, Germany
[b]Institute for Technical und Macromolecular Chemistry, RWTH Aachen University, 52074 Aachen, Germany
[c]Ruhr University Bochum, Universitätsstr. 150, 44801 Bochum, Germany.

Abstract: Colloidal and supported manganese nanoparticles were synthesized following an organometallic approach and applied in the catalytic transfer hydrogenation (CTH) of aldehydes and ketones. Reaction parameters for the preparation of colloidal nanoparticles (NPs) were optimized to yield small (2-2.5 nm) and well-dispersed NPs. Manganese NPs were further immobilized on an imidazolium-based supported ionic phase (SILP) and characterized to evaluate NP size, metal loading, and oxidation states. Oxidation of the Mn NPs by the support was observed resulting in an average formal oxidation state of +2.5. The MnO$_x$@SILP material showed promising performance in the CTH of aldehydes and ketones using 2-propanol as a hydrogen donor, outperforming previously reported Mn NPs-based CTH catalysts in terms of metal loading-normalized turnover numbers. Interestingly, MnO$_x$@SILP were found to lose activity upon air exposure, which correlates with an additional increase in the average oxidation state of Mn as revealed by X-ray absorption spectroscopic studies.

Table of Contents

1. Experimental Procedures

1.1. General and Safety Warning

High-pressure experiments with compressed $H_2(g)$ must be carried out only with appropriate equipment and under rigorous safety precautions.

1.2. Materials

Reactions involving water or oxygen-sensitive compounds are conducted under inert atmosphere (argon) using general Schlenk techniques and glove boxes. After synthesis, all materials were stored under argon. The used solvents were distilled, degassed, dried over molecular sieves (4 Å) and stored under argon. H_2 and Ar (purity > 99.999%) were provided by Westfalen AG. SiO_2 (Merck Grade 10184, pore size 100, 63–200 mm) was dehydroxylated in vacuo at 500 °C for 16 h prior to use. Imidazolium-based SILP was synthesized according to previously reported methods.[1]

Table S1. Used chemicals with their corresponding supplier.

Chemical	Supplier
Acetophenone	Alfa Aesar Thermo Fisher GmbH
Benzaldehyde	Alfa Aesar Thermo Fisher GmbH
tert-Butanol	Sigma-Aldrich Chemie GmbH
4-Chlorobenzaldehyde	Sigma-Aldrich Chemie GmbH
trans-Cinnamaldehyde	Sigma-Aldrich Chemie GmbH
4-Fluorobenzaldehyde	Sigma-Aldrich Chemie GmbH
Furfural	Sigma-Aldrich Chemie GmbH
Furfuralacetone	Synthesized in work group
Hexadecylamine	Sigma-Aldrich Chemie GmbH
LiHMDS	Sigma-Aldrich Chemie GmbH
Mesitylene	Alfa Aesar Thermo Fisher GmbH
4-Methoxybenzaldehyde	ABCR GmbH
4-Methylbenzaldehyde	ABCR GmbH
$MnCl_2 \cdot 4H_2O$	Sigma Aldrich
$[Mn[N(SiMe_3)_2]_2(THF)]$	Synthesized in work group
2-Nonanone	Sigma-Aldrich Chemie GmbH
Palmitic acid	Sigma-Aldrich Chemie GmbH
Phenylacetylene	Sigma-Aldrich Chemie GmbH
2-Propanol	Carl Roth GmbH + Co. KG
2-Propanol-d_8	ABCR GmbH
Triphenylphosphine	Alfa Aesar Thermo Fisher GmbH

1.3. Analytics

Gas chromatography-mass spectrometry (GC-MS) was performed on a *Shimadzu GCMS-QP2020* equipped with a CP-Wax 52 CB column (length: 60 cm, inner diameter: 0.25 mm, particle size: 0.25 µm) or an RTX-1 column (length: 30 cm, inner diameter: 0.25 mm, particle size: 0.5 µm). Transmission electron microscopy was performed on a *Hitachi HF2000 Cold FEG* operated at 200 kV. NMR spectroscopy measurements were carried out using a Bruker AVANCE NEO 400-spectrometer (^{1}H: 400 MHz). All measurements were conducted at ambient temperature. The chemical shift is given in ppm (parts per million) and the residual solvent signals were

referenced to tetramethyl silane (TMS) as internal standard for ^{1}H NMR spectroscopy. Inductively coupled plasma – mass spectrometry (ICP-MS) was conducted on a Shimadzu ICPMS-2030.

The Mn K-edge XAS measurements of MnO$_x$@SILP were performed at the P65 beamline of PETRA III (Germany).[2] At the P65 beamline, the X-ray beam was generated using the 5th order harmonic radiation from an 11-period undulator. A water-cooled fixed-exit Si(111) double crystal monochromator (DCM) was used to monochromatize the X-ray beam (energy resolution ΔE/E = 1.4 × 10^{-4}). The DCM was operated in QEXAFS mode, and the undulator offset to the DCM was calibrated to have the maximum photon flux. The X-ray beam was focused and collimated at the sample position to a spot size of approximately 1.0 mm × 0.5 mm (H × V). XAS spectra from 6345 eV to 7345 eV were collected in fluorescence mode using a 4-element silicon drift detector. The energy of the incident beam was calibrated by assigning the energy of the first inflection in the first derivative XAS of Mn foil to 6539 eV. The intensity of the incident beam (I_0) was monitored by ionization chamber. The sample powder was sealed inside a PEEK powder cell using Kapton tapes and transferred to the beamline anaerobically in a liquid N_2 Dewar. The XAS of the MnO$_x$@SILP were measured in a liquid He cryostat at 15 K. 10 repetitions of XAS scans were collected and merged to improve the signal to noise ratio.

The Mn K-edge XAS measurements of MnO$_x$@SILP_Air and the gradual oxidation process of MnO$_x$@SILP were carried out at the B18 beamline of Diamond Light Source (UK).[3-4] B18 beamline is equipped with a bending magnet as the source of the X-rays. A fixed exit Si(111) DCM (energy resolution ΔE/E = 1.4 × 10^{-4}) was operated in QEXAFS mode which is optimized for continuous scanning. The monochromatic X-ray beam was focused using Pt coated mirrors, and a pair of Pt coated harmonic rejection mirrors was inserted in the beam path. The beam spot size on the sample is about 1.0 mm × 1.0 mm (H × V). XAS spectra from 6340 eV to 7390 eV were collected in fluorescence mode using a 4-element silicon drift detector. The energy of the incident beam was calibrated by assigning the energy of the first inflection in the first derivative XAS of Mn foil to 6539 eV. The intensity of the incident beam (I_0) was monitored by ionization chamber. The powder of MnO$_x$@SILP_Air was sealed inside a PEEK powder cell using Kapton tapes and measured under air at room temperature. 10 repetitions of XAS scans were collected and merged to improve the signal to noise ratio.

The Mn K-edge XAS spectra were analyzed using the Demeter software package (including Athena and Artemis programs, version 0.9.26).[5] Pre-edge background subtraction and post-edge normalization of the XAS data were performed using the Athena program. A linear regression background in the range of 6347 to 6517 eV was determined and a quadratic polynomial regression for post-edge normalization in the range of 6647 to 7345 eV was applied. The spectra were splined from k = 0 Å^{-1} to k = 14.4 Å^{-1} with rbkg of 1.0 and k-weight of 2. The fitting of EXAFS spectra (R range: 1 to 3.5 Å, k range: 3 to 11.5 Å^{-1}) was performed using the Artemis program based on scattering paths generated from FEFF6. The amplitude reduction factor S_0^2 is determined to be 0.9 by fitting of k^2-weighted R-space EXAFS of MnO based on the standard crystal parameters of MnO and was used as fixed parameter for the EXAFS fitting of other Mn samples.

1.4. Synthesis of [Mn(N(SiMe$_3$)$_2$)$_2$(THF)] (adapted from [6])

MnCl$_2$·4H$_2$O was dried *in vacuo* overnight at 210 °C and transferred into a glovebox. MnCl$_2$ (10.7 g, 85.3 mmol) was suspended in THF (90 mL) und refluxed for 5 h under Ar. The solvent was removed by filtration and the resulting [MnCl$_2$(THF)$_2$] was washed with THF (10 mL) and dried *in vacuo*. [MnCl$_2$(THF)$_2$] (5.36 g, 20 mmol) and LiHMDS (6.70 g, 40 mmol) were dissolved in THF (50 mL) and refluxed under Ar for 5 h. THF was removed *in vacuo*. The residue was suspended in pentane (10 mL) and the formed LiCl was filtered off over celite. The product was purified by distillation, yielding [Mn(N(SiMe$_3$)$_2$)$_2$(THF)] as a rose solid.

1.5. Synthesis of colloidal Mn NPs

A solution of [Mn[N(SiMe$_3$)$_2$]$_2$(THF)] in mesitylene (1.0 mL) was combined with a solution of the used ligand(s) in mesitylene (1.0 mL) in a Fischer-Porter bottle. The Fischer-Porter bottle was evacuated and backfilled with H$_2$ and the suspension was stirred under H$_2$ (3 bar) at *T* °C for *t* h. After reaction, the Fischer-Porter bottle was evacuated and refilled with Ar. Samples were stored in a glove box.

1.5.1. Exemplary synthesis of colloidal Mn NPs (Table 1, Entry 3)

A solution of [Mn[N(SiMe$_3$)$_2$]$_2$(THF)] (20 mg, 0.0447 mmol) in mesitylene (1.0 mL) was combined with a solution of hexadecylamine (10.8 mg, 0.0447 mmol) in mesitylene (1.0 mL) in a Fischer-Porter bottle. The Fischer-Porter bottle was evacuated and backfilled with H$_2$ and the suspension was stirred under H$_2$ (3 bar) at 150 °C for 18 h. After reaction, the Fischer-Porter bottle was evacuated and refilled with Ar. The sample was stored in a glovebox.

1.6. Synthesis of MnO$_x$@SILP and MnO$_x$@SiO$_2$

[Mn[N(SiMe$_3$)$_2$]$_2$(THF)] (89.6 mg, 0.2 mmol) was dissolved in mesitylene (4.0 mL) and added to a Fischer-Porter bottle (70 mL). The imidazolium-based SILP or SiO$_2$ (500 mg) was added to the solution along with mesitylene (1.0 mL), and the suspension was stirred under argon at r.t. for 30 min. The Fischer-Porter bottle was evacuated and backfilled with H$_2$ and the suspension was stirred under H$_2$ (3 bar) at 150 °C for 18 h. The supernatant was removed and the material was washed with toluene (3 x 5.0 mL) and dried *in vacuo* at 45 °C for 1 h.

1.7. Catalytic transfer hydrogenation reactions

In a typical experiment, the substrate (0.2 mmol, 25 equiv.) and MnO$_x$@SILP (20.7 mg, 0.008 mmol Mn, 1 equiv.) were weighed into a glass inlet of a 10 mL autoclave in a glovebox. 2-propanol (2 mL) was added and the reaction mixture was stirred at 170 °C for 18 h under an atmosphere of Ar in a pre-heated aluminum heating cone. After reaction, the autoclave was cooled in a water bath and the reaction mixture was filtered into a GC vial for characterization, adding tetradecane as internal standard. Conversions and selectivities were determined *via* GC-FID.

2. Supplementary Tables and Figures

Table S2. Fitting results of Mn K-edge k^2-weighted EXAFS spectra for Mn samples.

Sample	Scattering path	Amp	C.N.	R [Å]	σ^2 [Å^2]	ΔE_0 [eV]	R-factor
MnO	Mn-O	0.9 ± 0.1	6 (fixed)	2.19 ± 0.01	0.0103 ± 0.0022	0.9 ± 0.1	0.0109
	Mn-Mn		12 (fixed)	3.14 ± 0.01	0.0101 ± 0.0011		
MnO$_x$@SILP (1)	Mn-O	0.9 (fixed)	1.2 ± 0.2	1.93 ± 0.02	0.0070 ± 0.0013	0.2 ± 1.1	0.0078
	Mn-O		2.5 ± 0.3	2.15 ± 0.01			
	Mn-Mn		1.1 ± 0.3	3.18 ± 0.02	0.0141 ± 0.0027		
MnO$_x$@SILP (2)	Mn-N	0.9 (fixed)	1.6 ± 0.3	1.94 ± 0.02	0.0051 ± 0.0019	-1.8 ±1.3	0.0091
	Mn-O		2.2 ± 0.3	2.13 ± 0.01			
	Mn-Si		0.9 ± 0.4	3.39 ± 0.02	0.0061 ± 0.0048		
MnO$_x$@SILP_Air	Mn-O	0.9 (fixed)	2.7 ± 0.3	1.91 ± 0.01	0.0073 ± 0.0010	-1.8 ± 1.4	0.0170
	Mn-O		1.9 ± 0.3	2.21 ± 0.01			
	Mn-Mn		1.3 ± 0.1	2.83 ± 0.02			
	Mn-Mn		2.4 ± 0.4	3.07 ± 0.02	0.0146 ± 0.0021		
	Mn-Mn		2.4 ± 0.4	3.71 ± 0.03			

C.N. = coordination number; R = interatomic distance; σ^2 = Debye-Waller factor. ΔE_0 = energy shift refers to the E_0 position in the EXAFS fitting model. The fitting errors of C.N. are mathematically calculated by Artemis program. Due to the strong correlation between C.N. and σ^2, the actual errors of C.N. would be affected by the uncertainties of the σ^2 values and be bigger than the program estimated values. The amplitude reductio factor (0.9) is determined by fitting of the EXAFS spectra of MnO using two single scattering paths for the first and second coordination shells respectively, and the value is used as fixed parameter for the EXAFS fitting of other Mn samples.

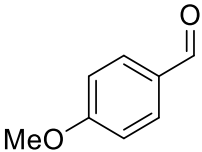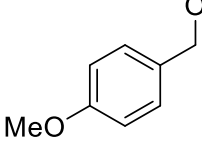**Table S3.** FEFF-calculated coordination number and bond length of reference manganese materials.[a]
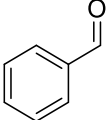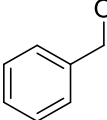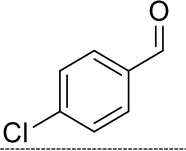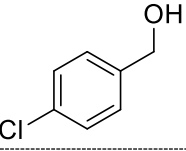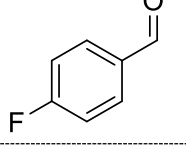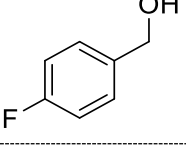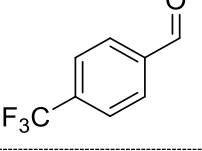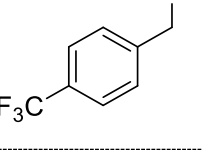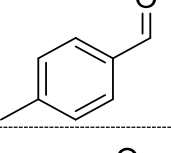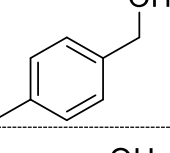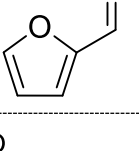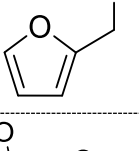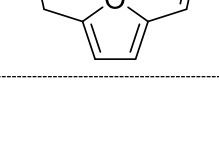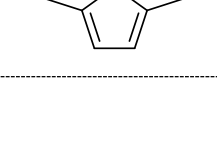
Compound	Space Group	Scattering Path	C.N.	R [Å]	Database & Index
C$_{20}$H$_{52}$MnN$_2$O$_2$Si$_4$	$P2_1/c$	Mn-N	2	2.038	CCDC: 837191
		Mn-O	2	2.217	
		Mn-Si	2	3.167	
		Mn-Si	2	3.267	
MnO	$Fm\bar{3}m$	Mn-O	6	2.222	COD: 9008674
		Mn-Mn	12	3.143	
Mn$_3$O$_4$	$I4_1/amd$	Mn(1)-O	4	2.040	COD: 1514115
		Mn(1)-Mn(2)	8	3.432	
		Mn(1)-O	8	3.475	
		Mn(1)-Mn(1)	4	3.726	
		Mn(1)-Mn(2)	4	3.823	
		Mn(2)-O	4	1.930	
		Mn(2)-O	2	2.282	
		Mn(2)-Mn(2)	2	2.882	
		Mn(2)-Mn(2)	4	3.119	
		Mn(2)-Mn(1)	4	3.432	
		Mn(1)-Mn(2)	2	3.823	
Mn$_2$O$_3$	$Ia\bar{3}$	Mn(1)-O	6	2.015	COD: 8103497
		Mn(1)-Mn(2)	6	3.139	
		Mn(1)-Mn(2)	6	3.526	
		Mn(2)-O	2	1.830	
		Mn(2)-O	2	1.957	
		Mn(2)-O	2	2.265	
		Mn(2)-Mn(1)	2	3.139	
		Mn(2)-Mn(2)	4	3.151	

		Mn(2)-Mn(1)	2	3.526	
		Mn(2)-Mn(2)	4	3.537	
MnO₂	$P4_2/mnm$	Mn-O	6	1.878	COD: 9009081
		Mn-Mn	2	2.871	
----		Mn-O	4	3.343	
		Mn-Mn	8	3.424	

[a]Crystal structural parameters are retrieved from the ICSD (Inorganic Crystal Structure Database, https://icsd.products.fiz-karlsruhe.de/), COD (Crystal Open Database, http://www.crystallography.net/) and CCDC (Cambridge Crystallographic Data Centre, https://www.ccdc.cam.ac.uk/). For Mn₂O₃ crystal, there are two types of Mn sites in the structure, labeled as Mn(1) and Mn(2) respectively. The ratio between the two Mn sites in the structure is 1:3. For Mn₃O₄ crystal, there are two types of Mn sites in the structure, labeled as Mn(1) and Mn(2) respectively. The ratio between the two Mn sites in the structure is 3:8.

Table S4. Optimization of reaction conditions for the CTH of aldehydes and ketones using MnOₓ@SILP.

Entry	Substrate	Product	T [°C]	X [%]	Y [%]	S [%]
1			170	98	98	> 99
2			170	> 99	75	75
3			150	66	61	91
			170	> 99	> 99	> 99
4			170	44	44	> 99
			200	> 99	> 99	> 99
5			120	54	54	>99
			170	98	98	>99
6			170	85	30	35
7			120	77	77	> 99
			150	82	82	> 99
			170	87	87	> 99
8			120	71	65	92
			170	>99	71	71

Entry	Substrate	Product	T	X	Y	S
9	(E)-cinnamaldehyde	cinnamyl alcohol	120	61	61	> 99
			150	> 99	> 99	> 99
			170	> 99	> 99	> 99
10	furyl butenone	furyl butenol	120	60	56	93
			170	84	68	81
11	$CH_3CO\text{-}C_7H_{15}$	$CH_3CH(OH)\text{-}C_7H_{15}$	170	60	60	> 99
12	acetophenone	1-phenylethanol	170	74	74	> 99
			170[a]	76	76	> 99
			200	86	30	35

Reaction conditions: Substrate (0.2 mmol, 25 equiv.), MnO$_x$@SILP (20.7 mg, 0.008 mmol metal), 18 h, T °C, 700 rpm, 2-propanol (2.0 mL); yields were determined by GC-FID using tetradecane as internal standard. [a] Reaction time = 24 h. X = conversion, Y = yield, S = selectivity.

Table S5. Conversions, yields, and selectivities of the CTH of 1 to 1a with 2-propanol using MnO$_x$@SILP exposed to air and under oxygen-free conditions.

t [h]	Exposed to air	Conversion [%]	Selectivity [%]
4	✗	44	>99
4	✓	11	>99
18	✗	98	>99
18	✓	27	>99

Reaction conditions: MnO$_x$@SILP or MnO$_x$@SILP_air (20.7 mg, 0.008 mmol metal), 25 eq. substrate, 150 °C, t h, 700 rpm, 2-propanol (2.0 mL); yields were determined by GC-FID using tetradecane as internal standard.
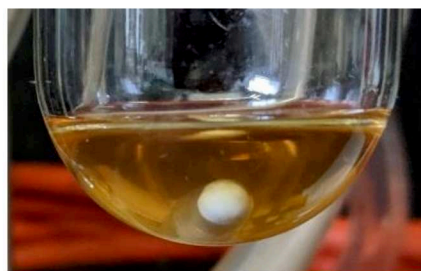
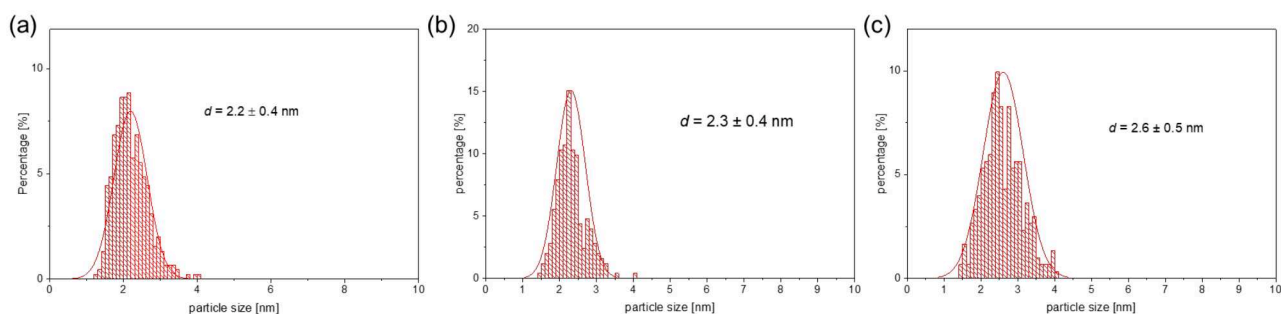**Figure S1.** Photograph of the resulting solution of Entry 4 in Table 1.

Figure S2. Size distribution of NPs prepared according to Table 1, (a) Entry 3: 1 eq HDA (number of particles measured n = 407), (b) Entry 7: 1.5 eq HDA, (n = 252) and (c) Entry 14: 1 eq HDA, 5 times higher Mn concentration (n = 311).
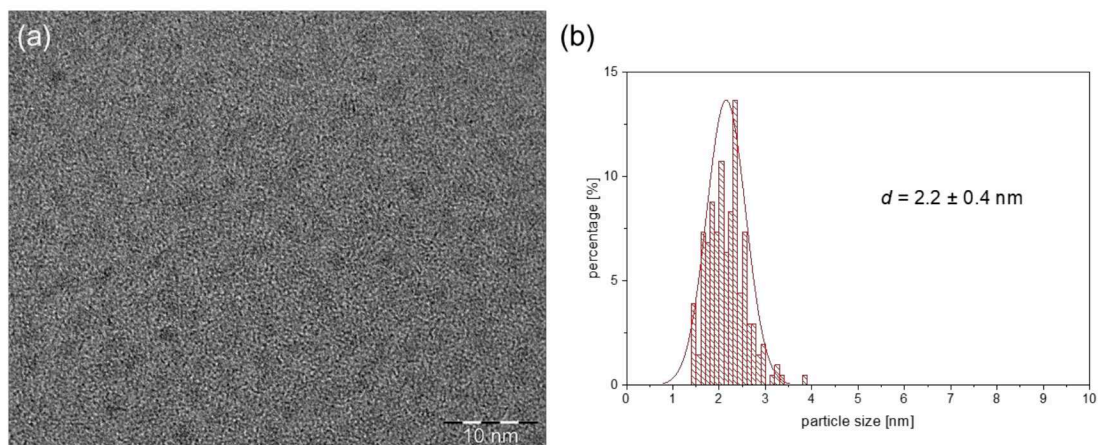
Figure S3. (a) TEM image of colloidal Mn NPs (see conditions Table 1, Entry 8) and (b) NP size distribution of n = 205 particles.
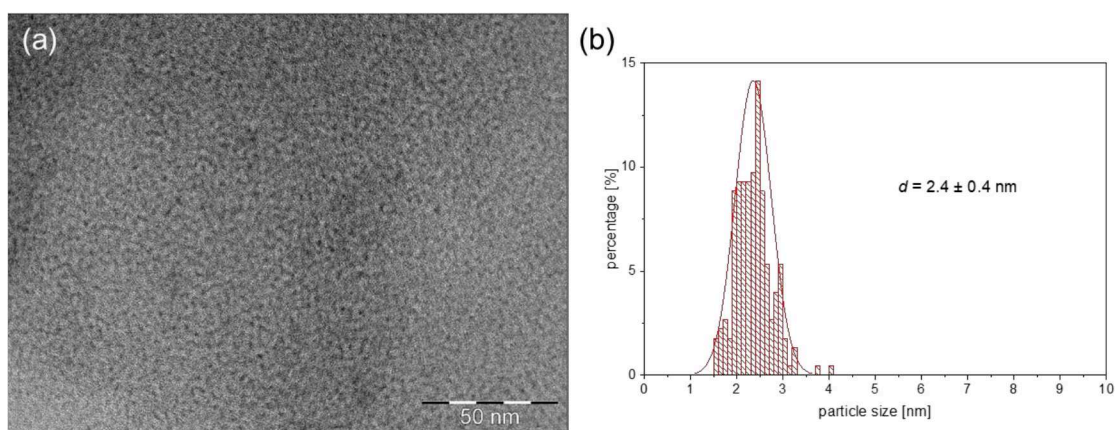

Figure S4. (a) TEM image of colloidal Mn NPs (see conditions Table 1, Entry 9) and (b) NP size distribution of n = 226 particles).
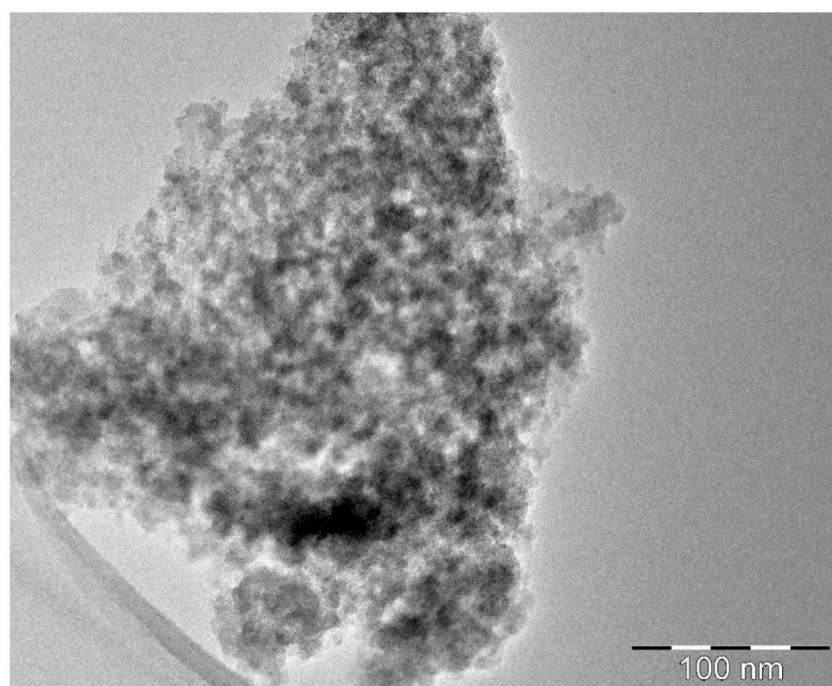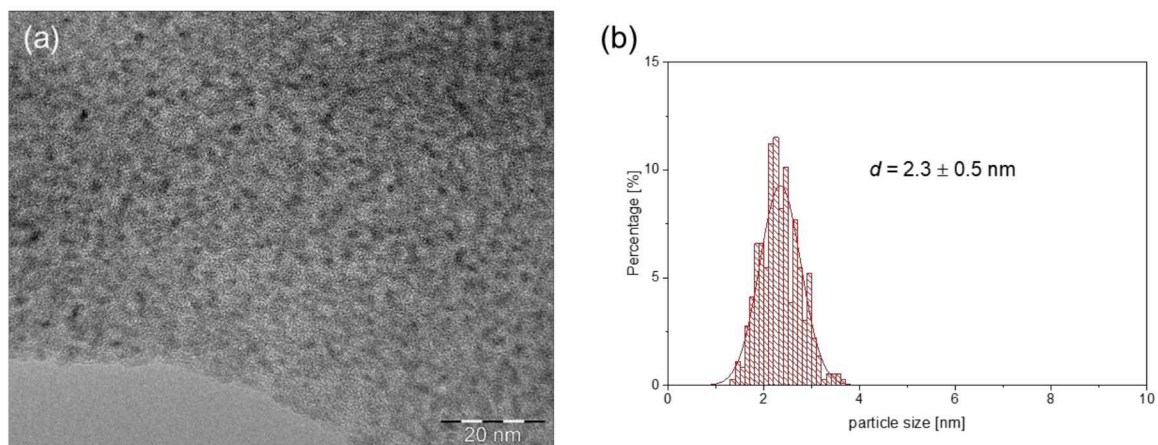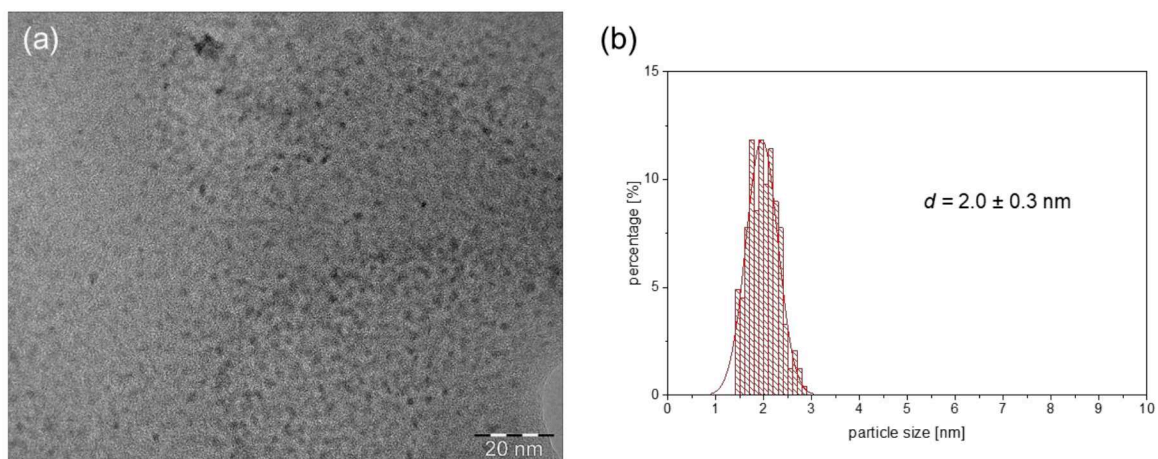

Figure S5. TEM image of aggregated Mn NPs (see conditions Table 1, Entry 11).

Figure S6. (a) TEM image of colloidal Mn NPs (see conditions Table 1, Entry 12) and (b) NP size distribution of n = 365 particles.

Figure S7. (a) TEM image of colloidal Mn NPs (Table 1, entry 13) and (b) NP size distribution of n = 245 particles.
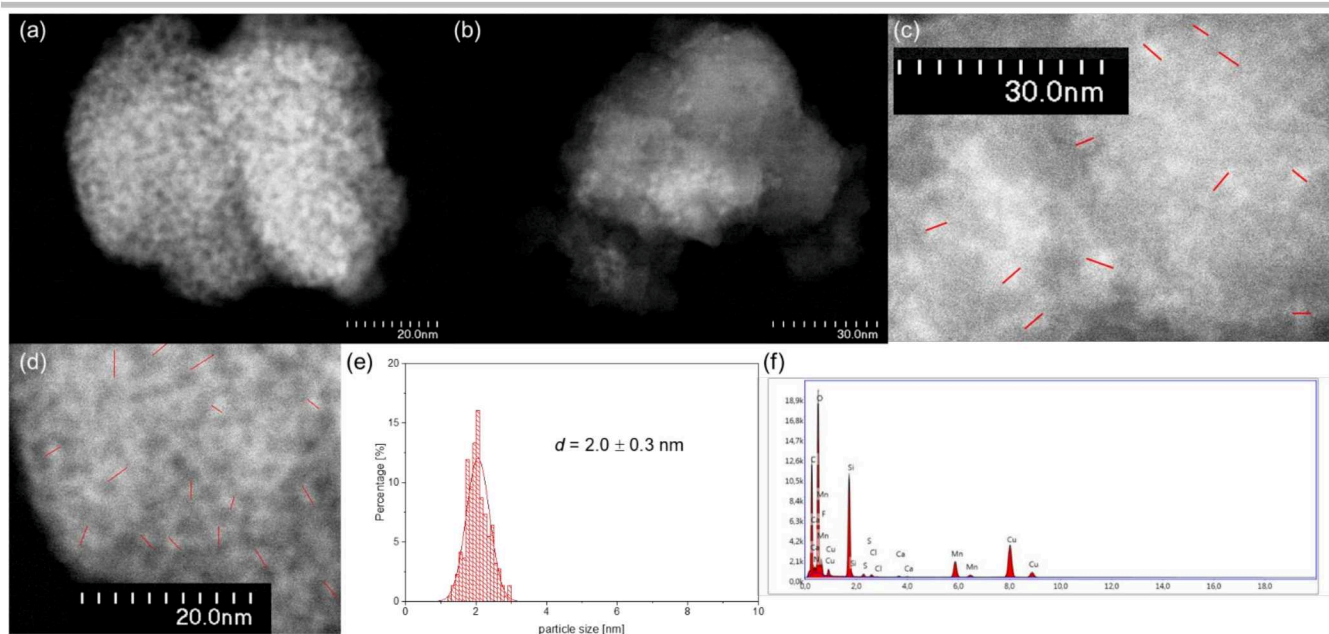
Figure S8. (a)-(d) Additional STEM-HAADF images of MnO$_x$@SILP with (c)-(d) indicated NPs. (e) NP size distribution of n = 218 particles of MnO$_x$@SILP and (f) EDX spectrum (sum spectrum) for the STEM-HAADF image of MnO$_x$@SILP (Figure 4).
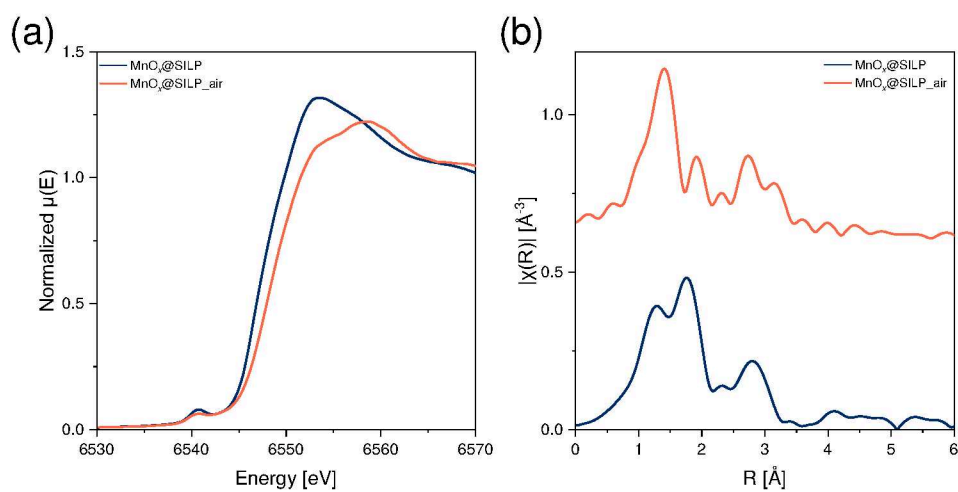

Figure S9. (a) Normalized XANES spectra of MnO$_x$@SILP and MnO$_x$@SILP_air. (b) k^2-weighted R-space EXAFS spectra of MnO$_x$@SILP and MnO$_x$@SILP_air. The spectra are plotted without phase correction.
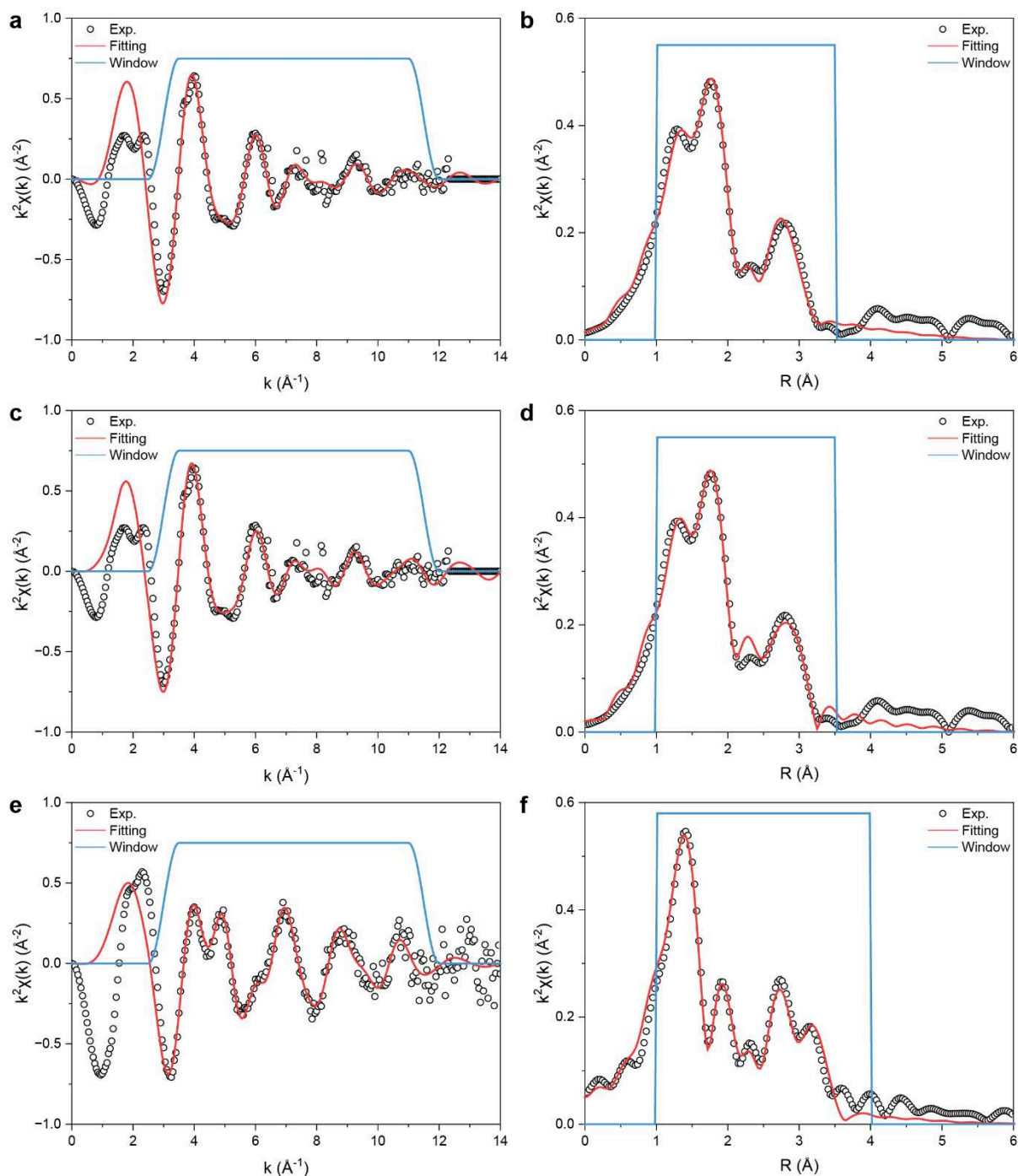
Figure S10. Fitting results of Mn K-edge k^2-weighted EXAFS spectra for Mn samples. (a, b) k-space and R-space EXAFS spectra of MnO_x@SILP using Mn-Mn scattering path for the second coordination shell. (c, d) k-space and R-space EXAFS spectra of MnO_x@SILP using Mn-Si scattering path for the second coordination shell. (e, f) k-space and R-space EXAFS spectra of MnO_x@SILP after exposed to air. The experimental data, fitted spectra and fitting window are plotted as black circles, red curves and blue curves.
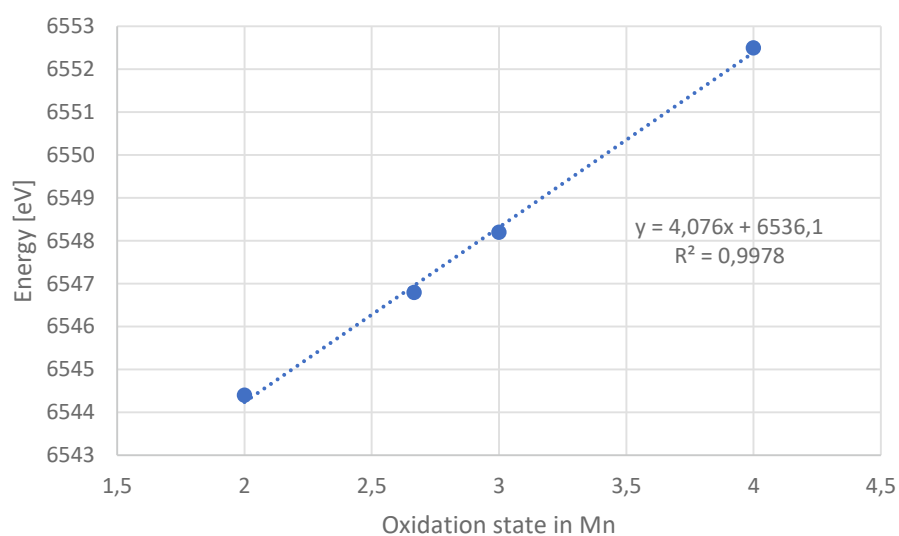
Figure S11. Correlation of the oxidation state of Mn reference materials (from left to right: MnO, Mn_3O_4, Mn_2O_3, MnO_2) to the position of the first maximum after their pre-edge.
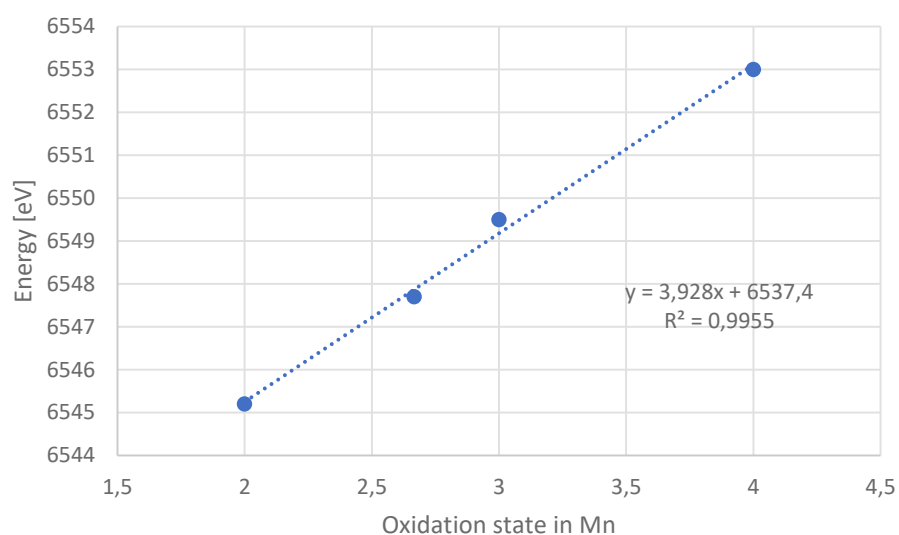

Figure S12. Correlation of the oxidation state of Mn reference materials (from left to right: MnO, Mn_3O_4, Mn_2O_3, MnO_2) to the position of the half-edge jump.
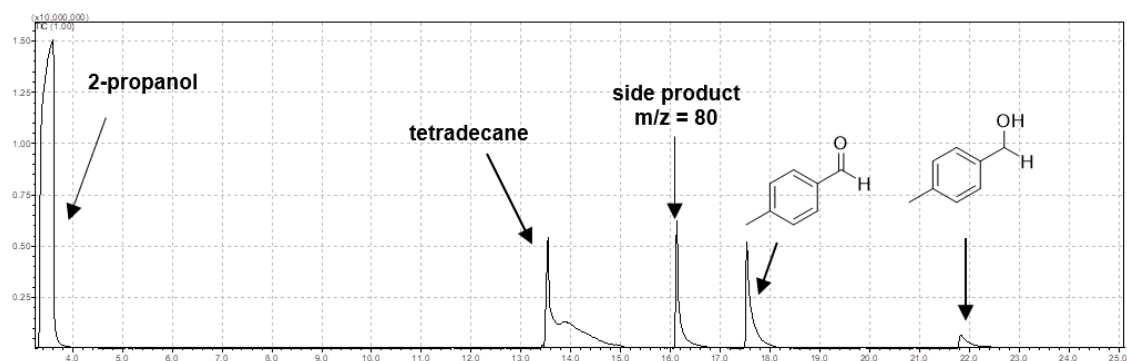

Figure S13. GC-MS spectrum of the reaction solution obtained after the CTH of 4-methylbenzaldehyde with 2-propanol using MnO$_x$@SILP. Reaction conditions: Substrate (24.9 mg, 0.2 mmol, 25 equiv.), MnO$_x$@SILP (20.7 mg, 0.008 mmol Mn, 1 equiv.), 18 h, 170 °C, 700 rpm, 2-propanol (2.0 mL).

WILEY-VCH

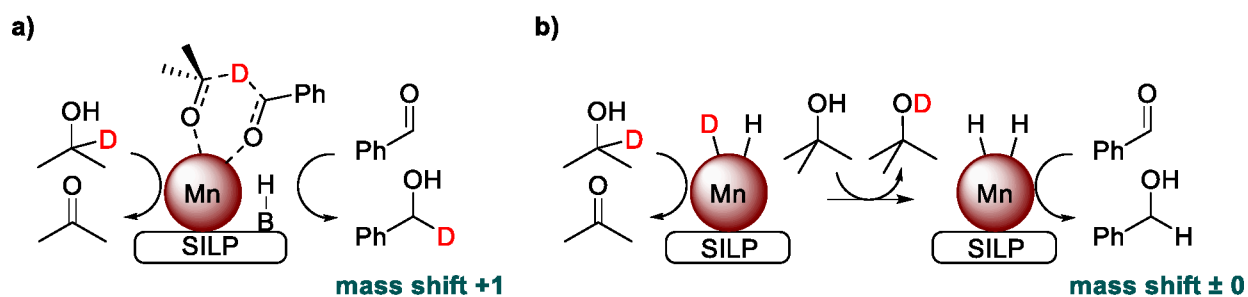**Figure S14.** (a) Possible reaction mechanism for the CTH of benzaldehyde using MnO$_x$@SILP, following an intermolecular hydrogen transfer. B = basic sites of the support. (b) CTH reaction mechanism following a metal-mediated hydrogenation step.[7]
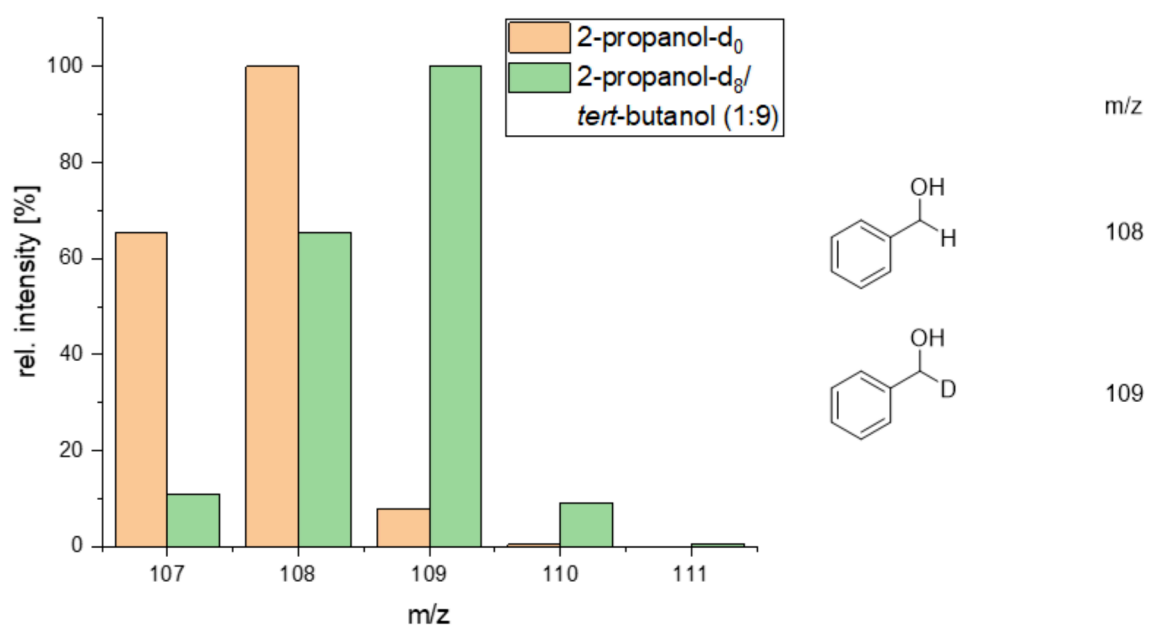

Figure S15. GC-MS spectra of the product of the CTH of benzaldehyde using MnO$_x$@SILP. Reaction conditions: Substrate (22.0 mg, 0.2 mmol, 25 equiv.), MnO$_x$@SILP (20.7 mg, 0.008 mmol Mn, 1 equiv.), 18 h, 170 °C, 700 rpm, 2-propanol-d$_0$ (2.0 mL) or a mixture of 2-propanol-d$_8$ (0.2 mL) and *tert*-butanol (1.8 mL).
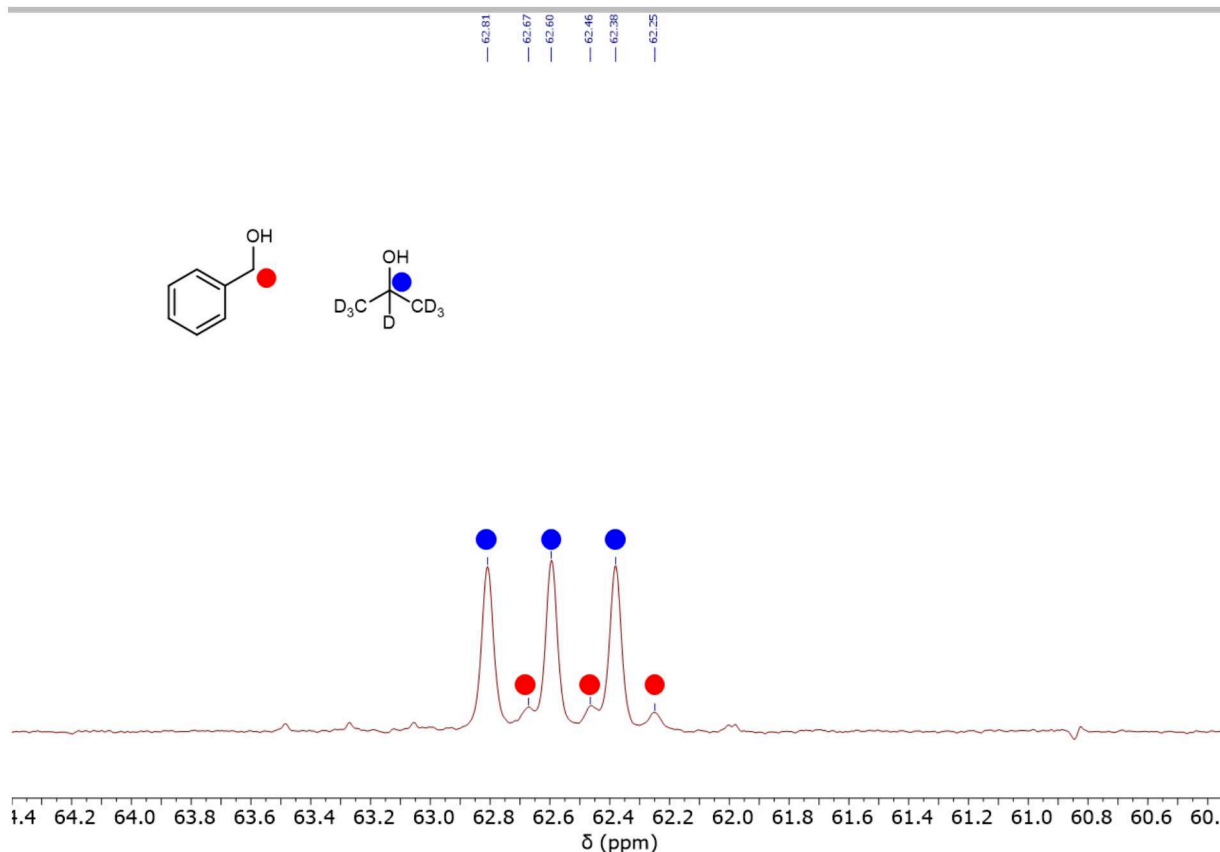
Figure S16. ^{13}C NMR spectrum (100 MHz, CD$_2$Cl$_2$) of the crude reaction mixture of the CTH of benzaldehyde in a mixture of 2-propanol-d$_8$/*tert*-butanol (1:9) after 18 h, 170 °C using MnO$_x$@SILP.

Figure S17. ^{1}H NMR spectra (400 MHz, CDCl$_3$) of a) 2-propanol-d$_0$ and b) a mixture of 2-propanol-d$_8$/*tert*-butanol (1:9) after 18 h, 170 °C in the presence of MnO$_x$@SILP, showing no H-D exchange at the C-D groups of 2-propanol d$_8$.

Figure S18. ^{1}H NMR spectrum (400 MHz, CD$_2$Cl$_2$) of the crude reaction mixture of the CTH of benzaldehyde in a mixture of 2-propanol-d$_8$/*tert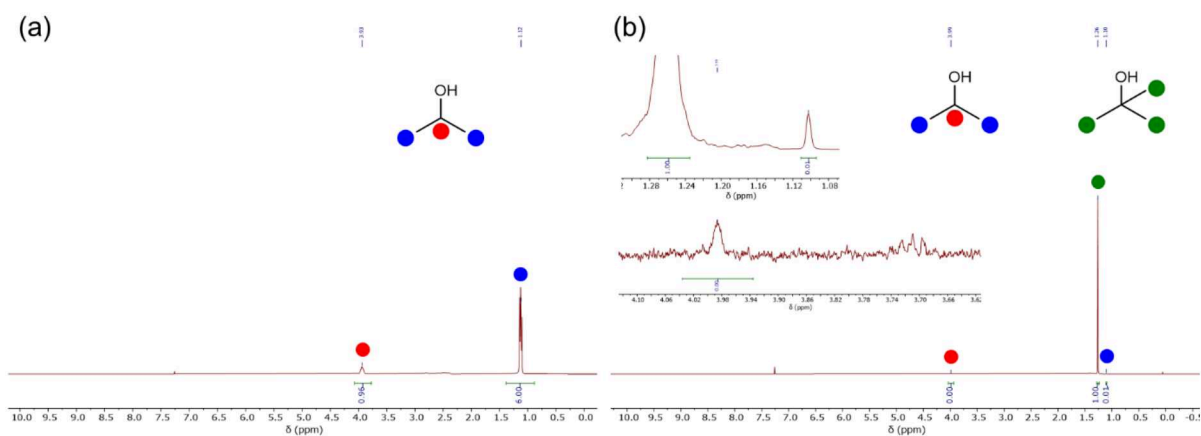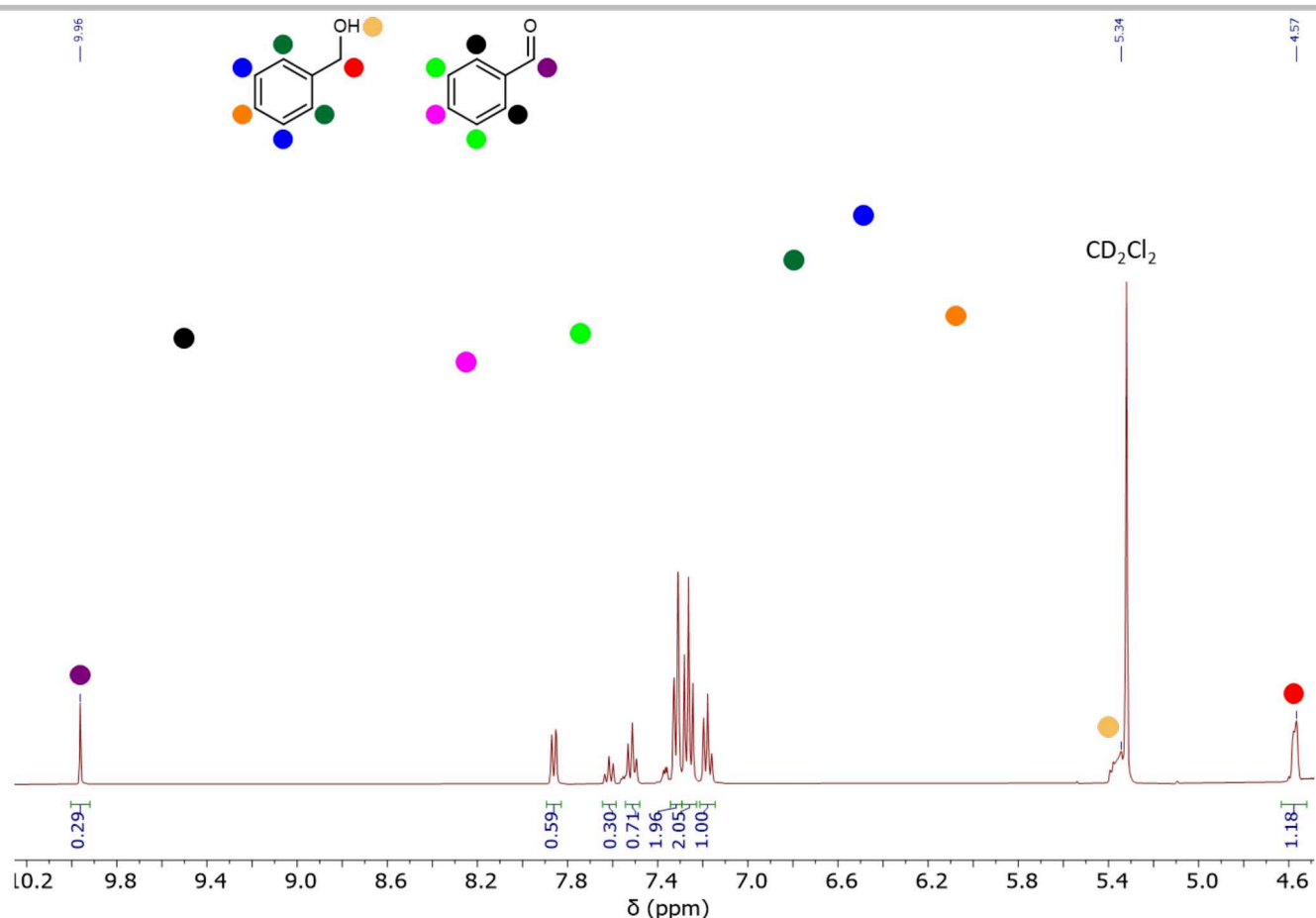*-butanol (1:9) after 18 h, 170 °C using MnO$_x$@SILP. Under these conditions, a mixture of benzyl alcohol and unreacted benzaldehyde is yielded. The area of the CH$_2$-group of benzyl alcohol (red) is approximately half of the expected value, showing the incorporation of D during the CTH in that position. No H-D exchange occurred on the C-H group of the substrate (purple).
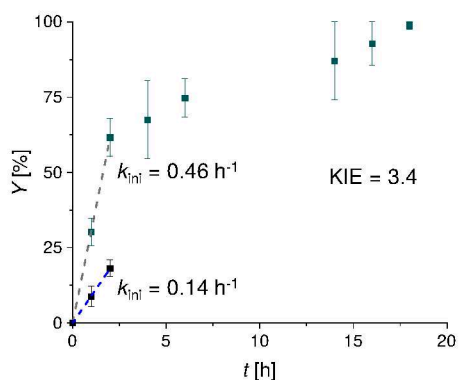

Figure S19. Time profiles for the CTH of **1** to **1a** using MnO$_x$@SILP as a catalyst using 2-propanol-d$_0$ or 2-propanol-d$_8$ as solvent to determine the kinetic isotope effect (KIE) over the initial reaction rates. Reaction conditions: MnO$_x$@SILP (20.7 mg, 0.008 mmol Mn), benzaldehyde (22.0 mg, 0.2 mmol, 25 equiv.), 170 °C, t h, 700 rpm, solvent (2.0 mL). Product selectivity to **1a** was >99% in all reactions. Yields were determined by GC-FID using tetradecane as an internal standard. Data points are average values of 2 to 3 experiments and error bars represent standard deviations.

3. References

[1] K. L. Luska, J. Julis, E. Stavitski, D. N. Zakharov, A. Adams, W. Leitner, *Chem. Sci.* **2014**, *5*, 4895– 4905.

[2] E. Welter, R. Chernikov, M. Herrmann, R. Nemausat, *AIP Conf. Proc.* **2019**, *2054*, 040002.

[3] A. J. Dent, G. Cibin, S. Ramos, S. A. Parry, D. Gianolio, A. D. Smith, S. M. Scott, L. Varandas, S. Patel, M. R. Pearson, L. Hudson, M. R. Pearson, L. Hudson, N. A. Krumpa, A. S. Marsch, P. E. Robins, *J. Phys.: Conf. Ser.* **2013**, *430* (1), 012023.

[4] A. J. Dent, G. Cibin, S. Ramos, A. D. Smith, S. M. Scott, L. Varandas, M. R. Pearson, N. A. Krumpa, C. P. Jones, P. E. Robbins, *J. Phys.: Conf. Ser.* **2009,** *190*, 012039.

[5] B. Ravel, M. Newville, *J. Synchrotron Radiat.* **2005**, *12* (4), 537-541.

[6] B. Horvath, R. Möseler, E. G. Horvath, *Z. anorg. Allg. Chem.* **1979**, *450*, 165-177.

[7] M. J. Gilkey, P. Panagiotopoulou, A. V. Mironenko, G. R. Jenness, D. G. Vlachos, B. Xu, *ACS Catal.* **2015**, *5*, 3988-3994.